Tetrahydrobenzo[*h*][1,6]naphthyridine–6-chlorotacrine hybrids as a new family of anti-Alzheimer agents targeting β-amyloid, tau, and cholinesterase pathologies

Ornella Di Pietro[a], F. Javier Pérez-Areales[a], Jordi Juárez-Jiménez[b], Alba Espargaró[c], M. Victòria Clos[d], Belén Pérez[d], Rodolfo Lavilla[e], Raimon Sabaté[c], F. Javier Luque[b,*], Diego Muñoz-Torrero[a,**]

[a] *Laboratori de Química Farmacèutica (Unitat Associada al CSIC), Facultat de Farmàcia, and Institut de Biomedicina (IBUB), Universitat de Barcelona, Av. Joan XXIII, 27-31, E-08028, Barcelona, Spain*

[b] *Departament de Fisicoquímica, Facultat de Farmàcia (Campus Torribera), and IBUB, Universitat de Barcelona, Prat de la Riba 171, E-08921, Santa Coloma de Gramenet, Spain*

[c] *Departament de Fisicoquímica, Facultat de Farmàcia, and Institut de Nanociència i Nanotecnologia (IN²UB), Universitat de Barcelona, Av. Joan XXIII, 27-31, E-08028, Barcelona, Spain*

[d] *Departament de Farmacologia, de Terapèutica i de Toxicologia, Institut de Neurociències, Universitat Autònoma de Barcelona, E-08193, Bellaterra, Barcelona, Spain*

[e] *Laboratori de Química Orgànica, Facultat de Farmàcia, Universitat de Barcelona, and Barcelona Science Park, Baldiri Reixac 10-12, E-08028, Barcelona, Spain*

* Corresponding author. Tel.: +34 934024557; fax: +34 934024539.

** Corresponding author. Tel.: +34 934024533; fax: +34 934035941.

E-mail addresses: fjluque@ub.edu (F. J. Luque), dmunoztorrero@ub.edu (D. Muñoz-Torrero).

ABSTRACT

Optimization of an essentially inactive 3,4-dihydro-2*H*-pyrano[3,2-*c*]quinoline carboxylic ester derivative as acetylcholinesterase (AChE) peripheral anionic site (PAS)-binding motif by double O → NH bioisosteric replacement, combined with molecular hybridization with the AChE catalytic anionic site (CAS) inhibitor 6-chlorotacrine and molecular dynamics-driven optimization of the length of the linker has resulted in the development of the trimethylene-linked 1,2,3,4-tetrahydrobenzo[*h*][1,6]naphthyridine–6-chlorotacrine hybrid **5a** as a picomolar inhibitor of human AChE (hAChE). The tetra-, penta-, and octamethylene-linked homologues **5b**–**d** have been also synthesized for comparison purposes, and found to retain the nanomolar hAChE inhibitory potency of the parent 6-chlorotacrine. Further biological profiling of hybrids **5a**–**d** has shown that they are also potent inhibitors of human butyrylcholinesterase and moderately potent Aβ42 and tau anti-aggregating agents, with IC_{50} values in the submicromolar and low micromolar range, respectively. Also, *in vitro* studies using an artificial membrane model have predicted a good brain permeability for hybrids **5a**–**d**, and hence, their ability to reach their targets in the central nervous system. The multitarget profile of the novel hybrids makes them promising leads for developing anti-Alzheimer drug candidates with more balanced biological activities.

Keywords: Tetrahydrobenzo[*h*][1,6]naphthyridines
Multitarget compounds
Dual binding site AChE inhibitors
Aβ aggregation inhibitors
Tau aggregation inhibitors

1. Introduction

Alzheimer's disease (AD) currently represents one of the most important unmet medical needs worldwide. Worryingly, because prevalence and mortality figures associated with AD will keep increasing, this condition will be even more pronounced in the upcoming decades, unless efficient disease-modifying drugs become available [1].

Current treatments for AD involve the use of acetylcholinesterase (AChE) inhibitors (donepezil, rivastigmine and galantamine) or NMDA receptor antagonists (memantine), which restore neurotransmitter deficits that are responsible for the symptomatic phase of the disease (cognitive, functional, and neuropsychiatric deficits) that appears a decade or more after the onset of the neurodegenerative process.

It is becoming increasingly apparent that the simultaneous modulation of several crucial targets that play early roles in the neuropathogenic process is a promising approach to derive effective drugs that can modify the course of AD [3,4]. Obviously, administration of these multitarget drugs depends on a precise knowledge of the timing of the critical neuropathologies to be hit and on the development of suitable biomarkers that enable timely therapeutic interventions and the assessment of their impact on AD progression. Whereas these important issues are addressed [2,5,6], the parallel development of multitarget drugs hitting different combinations of key biological targets should be actively pursued.

Neuropathologies related to the β-amyloid peptide (Aβ) and tau protein are thought to be at the root of the neurodegenerative process [2]. Also, AChE seems to play a role in the early phases of the disease, inasmuch as it can bind to Aβ, thereby accelerating its aggregation into oligomers and fibrils and increasing the neurotoxicity of Aβ aggregates [7]. The Aβ proaggregating action of AChE has been reported to reside in its peripheral anionic site (PAS) [7c], which is located at the mouth of a 20 Å deep gorge that leads to the catalytic anionic site (CAS) of the enzyme [8].

We have recently developed a new family of potent AChE inhibitors able to simultaneously bind at the CAS and PAS of the enzyme, i.e. dual binding site inhibitors, which were designed by molecular hybridization of the novel 3,4-dihydro-2*H*-pyrano[3,2-*c*]quinoline scaffold of ester **1** and the potent AChE CAS inhibitor 6-chlorotacrine, **2** (Fig. 1) [9]. The most potent hybrid of the series, compound **3** (Fig. 1) retained the high human AChE inhibitory activity of the parent 6-chlorotacrine (**3**: IC_{50} = 7 nM in human erythrocyte AChE; IC_{50} = 19 nM in human recombinant AChE (hAChE)), and additionally exhibited a potent inhibitory activity of human butyrylcholinesterase (hBChE) and a weak Aβ antiaggregating activity (29% inhibition of AChE-induced Aβ40 aggregation at 100 μM and 21% inhibition of self-induced Aβ42 aggregation at 50 μM) [9].

Please, insert here Fig. 1.

Even though the 5-(4-chlorophenyl)-3,4-dihydro-2*H*-pyrano[3,2-*c*]quinoline moiety of **3** might establish *π*–*π* stacking interactions with the aromatic PAS residues Trp286 and Tyr72 (hAChE numbering), concomitant to the interactions of the 6-chlorotacrine unit at the CAS, the 5-(4-chlorophenyl)-3,4-dihydro-2*H*-pyrano[3,2-*c*]quinoline ester **1**, used as synthetic precursor of **3**, was found to be essentially inactive as AChE inhibitor. With the aim of optimizing this tricyclic scaffold as a PAS-binding moiety, we recently designed a family of tetrahydrobenzo[*h*][1,6]naphthyridines, which mainly resulted from the substitution of the oxygen atom at position 1 of the 3,4-dihydro-2*H*-pyrano[3,2-*c*]quinoline system of ester **1** by an amine nitrogen atom [10]. The rationale behind this structural modification was that the increased basicity of the pyridine nitrogen atom would enable i) its protonation at physiological pH, and hence, ii) the establishement of cation–π interactions, apart from π–π stacking, with the aromatic PAS residues. Indeed, the most potent compound of the series, **4** (Fig. 1), resulting from a double O → NH bioisosteric replacement from ester **1** at position 1 and at the side chain in position 9, exhibited a nanomolar hAChE inhibitory activity (IC_{50} = 65 nM) [10]. Molecular dynamics (MD) simulations confirmed the expected binding of the tricyclic moiety of **4** at the AChE PAS (cation–π / π–π interactions with Trp286) and hydrogen bond between the protonated pyridine nitrogen atom and the hydroxyl group of the PAS residue Tyr72) as well as additional interactions of the amide function at position 9 with midgorge residues (hydrogen bond between the amide NH group and the hydroxyl group of Tyr124) [10].
Once the PAS-binding moiety had been optimized, we inferred that molecular hybridization with the CAS binder 6-chlorotacrine should provide further improvement of the AChE inhibitory activity. The disposition of the amide chain at position 9 of the tetrahydrobenzo[*h*][1,6]naphthyridine **4** along the midgorge, with its nitrogen atom at a distance of ~6 Å from the position occupied by the exocyclic amino group of tacrine in its complex with *Torpedo californica* AChE (Fig. 2) [11], suggested that a linker of 3 methylenes should be optimal to connect both moieties retaining all their interactions

with AChE residues all along the enzyme gorge. Thus, the tetrahydrobenzo[*h*][1,6]naphthyridine–6-chlorotacrine hybrid **5a** (Fig. 1) was rationally designed as a novel multiple-site AChE inhibitor, bearing optimized PAS-binding moiety and tether length.

Please, insert here Fig. 2.

Herein, we describe the synthesis of the tetrahydrobenzo[*h*][1,6]naphthyridine–6-chlorotacrine hybrid **5a** and its longer tetra-, penta-, and octa-methylene-linked homologues **5b–d**, the evaluation of their inhibitory activities against hAChE and hBChE, and the study of their binding mode to hAChE by MD simulations. To further expand the potential multitarget profile of hybrids **5a**–**d**, their inhibitory activities against the aggregation of Aβ42 and tau protein in intact *Escherichia coli* cells, as a simplified *in vivo* model of aggregation of amyloidogenic proteins, were also evaluated. Moreover, the brain penetration of these hybrids, and therefore the ability to reach their targets at the central nervous system (CNS), was assessed by a parallel artificial membrane permeation assay (PAMPA-BBB).

2. Results and discussion

2.1. Synthesis of the tetrahydrobenzo[h][1,6]naphthyridine–6-chlorotacrine hybrids

Apart from the rationally designed trimethylene-linked hybrid **5a**, we planned the synthesis of the longer tetra- and penta-methylene homologues **5b** and **5c**, still bearing relatively short linkers. We also envisioned the synthesis of the octamethylene-linked analogue **5d**, mainly for comparison with the octamethylene-linked 3,4-dihydro-2*H*-pyrano[3,2-*c*]quinoline-based hybrid **3**, to gain further insight into the effect of the O → NH bioisosteric replacement at position 1 of the tricyclic system, while keeping the same tether length.

For the synthesis of hybrids **5a**–**d**, we used as starting material the *N*-Boc-protected tetrahydrobenzo[*h*][1,6]naphthyridine **6**, readily available by a multicomponent Povarov reaction between 4-chlorobenzaldehyde, ethyl 4-aminobenzoate and *N*-Boc-3,4-dihydro-2*H*-pyridine under the catalysis of $Sc(OTf)_3$ in acetonitrile [12], followed by DDQ oxidation [13] of the resulting diastereomeric mixture of octahydrobenzo[*h*][1,6]naphthyridines [10]. Saponification of ester **6**, followed by treatment of the resulting carboxylate with an Et_2O solution of HCl afforded the corresponding carboxylic acid, which was isolated as the naphthyridine hydrochloride. Coupling of the carboxylic acid with the known aminoalkyltacrine derivatives **7a–d** [14], using HOBt and EDC in the presence of Et_3N in a 10:1 mixture EtOAc/DMF, followed by silica gel column chromatography purification afforded the expected *N*-Boc-protected amides, in some cases together with directly deprotected amides (**5a** and **5c**). Treatment of the *N*-Boc-protected amides with 4 M HCl in dioxane at room temperature afforded the target amides **5a–d** in 34-80% total overall yields from ester **6** (Scheme 1).

The novel tetrahydrobenzonaphthyridine–6-chlorotacrine hybrids **5a–d** were fully characterized in the form of dihydrochloride salts through their spectroscopic data (IR, ^1H and ^{13}C NMR) and HRMS and their purity was assessed by elemental analysis. The biological characterization was also performed with the dihydrochloride salts.

Please, insert here Scheme 1.

2.2. Acetylcholinesterase inhibition

2.2.1. Evaluation of AChE inhibitory activity

The inhibitory activity of the novel hybrids **5a–d** against hAChE was evaluated by the method of Ellman *et al.* [15]. The 3,4-dihydro-2*H*-pyrano[3,2-*c*]quinoline derivatives **1** and **3**, as well as 6-chlorotacrine, **2**, were also evaluated under the same assay conditions as reference compounds. Also, the reported activity of compound **4** [10] was considered for comparison purposes.

All the tetrahydrobenzonaphthyridine–6-chlorotacrine hybrids turned out to be very potent inhibitors of hAChE (Table 1). Indeed, in agreement with the rational design strategy, the trimethylene-linked hybrid **5a** was the most potent hAChE inhibitor of the series, exhibiting a surprising picomolar IC_{50} value (IC_{50} = 6.27 pM). The highly potent inhibitory activity of **5a** is indicative of the success of the rational design strategy, in terms of both the molecular hybridization and the optimization of the tether length. On the one hand, molecular hybridization has been successful because **5a** is roughly 1000-fold and >10000-fold more potent than the parent compounds 6-chlorotacrine, **2**, and **4**, respectively (Table 1). On the other hand, the MD-driven optimization of the tether length has been also successful, inasmuch the trymethylene-linked hybrid **5a** is much more potent than the tetra-, penta-, and octa-methylene-linked counterparts (>2000-fold more potent than **5b** and **5c** and >300-fold more potent than **5d**).

Please, insert here Table 1.

The O → NH bioisosteric replacement, which had proven to be successful in the optimization from the 3,4-dihydro-2*H*-pyrano[3,2-*c*]quinoline ester **1** to the tetrahydrobenzo[*h*][1,6]naphthyridine amide **4** [10], has been also successful in the corresponding hybrids with 6-chlorotacrine, the tetrahydrobenzo[*h*][1,6]naphthyridine-based hybrid **5d** being roughly 10-fold more potent than the 3,4-dihydro-2*H*-pyrano[3,2-*c*]quinoline-based hybrid **3**, with the same tether length (Table 1). Overall, hybrid **5a** constitutes one of the most potent noncovalent inhibitors of hAChE so far reported, even though a few examples of other picomolar or even femtomolar inhibitors of AChE have also been described [14a,16].

2.2.2. Binding mode within AChE: Molecular modelling studies

To shed light on the structural basis of the surprisingly high AChE inhibitory activity determined for compound **5a**, the binding mode to hAChE was explored by means of MD simulations, taking advantage of the X-ray crystallographic structure of the hAChE complex with huprine W (PDB entry 4BDT [17]). The initial pose of the ligand was guided by the structural information available for the binding mode of huprine X to *Torpedo californica* AChE (PDB entry 1E66 [18]), which matches well the structure of huprine W bound to hAChE, and by the recently reported binding mode of compound **4** [10].

The analysis of the 100 ns MD trajectory supported the structural integrity and stability of the ligand bound to the hAChE gorge. Thus, with the sole exception of a slight reorientation of the tetrahydrobenzo[*h*][1,6]naphthyridine moiety in the PAS, which was originated from a conformational change in the loop defined by residues 289–292, the RMSD of the ligand remained fully stable during the last 60 ns of the trajectory (Fig. S1, Supplementary Material). The hybrid **5a** establishes a complex network of interactions with the residues of the binding site (Fig. 3). As expected, the 6-chlorotacrine moiety was tightly bound in the CAS due to the cation–π interactions with the aromatic rings of Trp86 and Tyr337 (average distances of 3.9 Å between the indole or phenol rings and the aminoacridine unit) and the hydrogen bond of the protonated acridine nitrogen atom with the carbonyl oxygen of His447 (average distance of 2.9 Å). On the other hand, the tetrahydrobenzo[*h*][1,6]naphthyridine moiety was firmly stacked against Trp286, thus enabling the formation of a cation–π interaction between the protonated quinoline nitrogen atom and the indole ring of Trp286. The binding of this moiety was also assisted by transient hydrogen bond interactions between the NH group and the hydroxyl oxygen of Tyr72. The most remarkable finding concerns the interactions formed by the amide group in the tether, as the amide NH group is involved in a hydrogen bond with Asp74 (average distance of 3.6 Å), which is in turn hydrogen-bonded to the hydroxyl group of Tyr341 (average distance of 2.8 Å), while the amide carbonyl oxygen forms either direct or water-mediated interactions with the hydroxyl group of Tyr337 (average distance of 4.9 Å). As a further test, the binding free energy of compound **5a** was determined with the Solvated Interaction Energy (SIE) method [19], which relies on MM/PBSA calculations in conjunction with weighting scaling factors for the free energy components suitably parameterized to reproduce the experimental binding affinities for a diverse set of protein–ligand complexes. The SIE binding affinity obtained for compound **5a** is –12.5 kcal/mol (Table S1, Supplementary Material), which is 4 kcal/mol lower than that determined for compound **4** (–8.5 kcal/mol [10]), which is in agreement with the ~10^4 ratio between the IC_{50} values reported in Table 1.

These findings provide a basis to explain the abrupt change in inhibitory activity between compounds **5a** and **5b**, as the enlargement of the oligomethylene chain between tacrine and the amide group would disrupt the interactions with the midgorge residues. On the other hand, the amide group that is present in the tether of some tacrine–indole heterodimers reported by Muñoz-Ruiz *et al*. as picomolar AChE inhibitors was also suggested to participate in a complex network of interactions with midgorge residues [14a]. In the most potent tacrine–indole heterodimer the amide group, located at six methylene groups from the tacrine unit, was suggested to interact with Tyr124 and Tyr337. In hybrid **5a** the shortening of the chain to three methylenes enables the formation of a distinct interaction pattern with Asp74 and Tyr337. Overall, these findings reinforce the significant contribution played by the midgorge in complementing both PAS and CAS and modulating the affinity of AChE inhibitors.

Please, insert here Fig. 3.

2.3. Butyrylcholinesterase inhibition

BChE is partly responsible for acetylcholine hydrolysis and hence, for the cholinergic deficit of AD patients, especially in advanced stages of the disease, when the levels of AChE in CNS markedly decrease. Thus, BChE also represents a biological target of interest for AD treatment [20]. The BChE inhibitory activity of hybrids **5a–d** against hBChE was evaluated by the method of Ellman *et al.* [15].

The parent compounds 6-chlorotacrine, **2**, and **4** are selective inhibitors of hAChE, albeit still exhibiting a moderately potent hBChE inhibitory activity, with IC_{50} values in the submicromolar range. Not unexpectedly, hybrids **5a–d** were also more potent against hAChE than hBChE, displaying submicromolar IC_{50} values for hBChE inhibition (Table 1). In this case, molecular hybridization resulted in an increased hBChE inhibitory activity relative to the parent compound **4** (3–8-fold) but in a slightly decreased potency relative to 6-chlorotacrine, **2**, with the exception of hybrid **5a**, which was equipotent to 6-chlorotacrine.

The length of the linker has little influence on the hBChE inhibitory activity. Only a slight trend toward decreased potency with increased tether length was observed, the shorter homologue **5a** being 1.7-, 2.8-, and 2.4-fold more potent than the longer counterparts **5b**, **5c**, and **5d**, respectively. Finally, the O → NH bioisosteric replacement had little influence on the hBChE inhibitory activity, the octamethylene-linked 3,4-dihydro-2*H*-pyrano[3,2-*c*]quinoline- and tetrahydrobenzo[*h*][1,6]naphthyridine-based hybrids **3** and **5d** roughly displaying the same potency (Table 1).

2.4. Aβ42 and tau aggregation inhibition

The aggregation of the amyloidogenic proteins Aβ, especially the most aggregation-prone and neurotoxic 42 amino acid form thereof (Aβ42), and tau are widely thought to constitute early pathogenic events in AD, and hence, they are the target of many drug candidates purported to modify the natural course of the disease [21].

We have recently developed a new methodology for the evaluation of the effects of putative inhibitors on the aggregation and subsequent formation of insoluble inclusion bodies of any amyloidogenic protein that can be overexpressed in *E. coli* cells [22]. The method relies on monitoring the changes in the fluorescence of Thioflavin S (Th-S) that are produced upon binding to amyloid aggregates rich in β-sheet structures. Compounds that are able to cross the membranes of *E. coli* cells and inhibit the aggregation of overexpressed amyloidogenic proteins will lead to a decrease in the fluorescence of Th-S. This method is fast, simple and inexpensive, as it avoids the use of synthetic peptides.

We have successfully used this method for the evaluation of inhibitors of Aβ42 and tau aggregation. Interestingly, the results obtained in the screening of Aβ42 aggregation inhibitors correlated very well with the results previously reported from *in vitro* assays using synthetic peptides, thereby validating this methodology [22].

The inhibitory activity of hybrids **5a–d** against Aβ42 and tau aggregation was assessed using this methodology. In general, very similar results and SAR trends were found for both activities. At 10 μM, hybrids **5a–d** exhibited percentages of inhibition in the ranges 52–77% and 41–69% against Aβ42 and tau aggregation, respectively (Table 1). Molecular hybridization led to increased Aβ42 and tau anti-aggregating activities, hybrids **5a–d** being more potent than 6-chlorotacrine (5–7-fold more potent against Aβ42 aggregation and 30–50-fold more potent against tau aggregation). The parent compound **4** could not be tested in these assays, but in *in vitro* tests it had been found to be a weak inhibitor of Aβ42 aggregation (15% inhibition at 10 μM) [10], so presumably hybrids **5a–d** are also more potent than **4**.

The length of the linker seemed to have a subtle effect on Aβ42 and tau anti-aggregating activities. These activities slightly increased with the tether length so that the longer homologue **5d** was 1.5-fold more potent than the shorter counterpart **5a** for both activities. On the other hand, the O → NH bioisosteric replacement had a similar effect on both activities, the tetrahydrobenzo[*h*][1,6]naphthyridine-based hybrid **5d** being roughly 1.5-fold more potent than the 3,4-dihydro-2*H*-pyrano[3,2-*c*]quinoline-based hybrid **3** for Aβ42 and tau aggregation inhibition.

The parallel results obtained for these hybrids against both Aβ42 and tau aggregation further support the notion that diseases based on the pathological aggregation of one or several amyloidogenic proteins might share common mechanisms and might be confronted with common therapeutic interventions [23].

Overall, hybrids **5a–d** can be considered as moderately potent dual Aβ42 and tau anti-aggregating compounds, with IC_{50} values that must lie around or below 10 μM. Because these anti-aggregating activities have been determined without involving the presence of AChE, the high AChE inhibitory activity of hybrids **5a–d** cannot be responsible for their Aβ42 and tau anti-aggregating activities, which might be ascribed, instead, to a direct interaction with Aβ42 and tau. The precise mechanisms through which these hybrids bind Aβ42 and tau and/or exert their anti-aggregating activities are unknown, even though it has been reported that the presence of several aromatic moieties with extended π-conjugated systems (including biphenyls and phenyl-substituted benzoheteroaromatic systems, similar to the phenylquinoline moiety present in hybrids **5a–d**) may enable binding to Aβ42 [24].

The dual Aβ42 and tau anti-aggregating profile is of much interest for disease-modifying anti-Alzheimer agents. However, it must be recognized that the anti-aggregating activities of hybrids **5a–d** are not well balanced relative to their cholinesterase inhibitory activities, especially AChE and particularly in the case of its picomolar inhibitor **5a**, which represents an important issue in multitarget compounds.

2.5. Blood–brain barrier permeation assay

Anti-Alzheimer drug candidates, like any other CNS drug, must be able to efficiently enter into the brain, which requires a good ability to cross the blood–brain barrier (BBB) and a low P-glycoprotein efflux liability [25]. The large molecular weight of hybrids **5a–d** (>500) might compromise their ability to cross biological membranes, including BBB [26]. However, a number of distinct anti-Alzheimer hybrid compounds with molecular weights over 500 have shown good oral availability and/or brain permeability in ex vivo and in vivo studies in mice [27]. Indeed, the positive results obtained for the hybrids **5a–d** in the aggregation studies in *E. coli* cells were already indicative of their ability to cross biological membranes, but a more accurate determination of their ability to cross the BBB was necessary. In this light, the brain permeability of the hybrids **5a–d** was predicted using an *in vitro* model of passive transcellular permeation, namely the widely known PAMPA-BBB assay [28]. Thus, the *in vitro* permeability (P_e) through a lipid extract of porcine brain was determined using a mixture of phosphate-buffered saline (PBS)/EtOH (70:30). Assay validation was made by comparing the experimental and reported permeability values of 14 commercial drugs (Table S2, Supplementary Material), which provided a good linear correlation: P_e (exp) = 1.5010 P_e (lit) – 0.8618 (R^2 = 0.9199). Using this equation and the limits established by Di *et al.* for BBB permeation [28], the following ranges of permeability were established: P_e (10^{-6} cm s^{-1}) > 5.1 for compounds with high BBB permeation (CNS+); P_e (10^{-6} cm s^{-1}) < 2.1 for compounds with low BBB permeation (CNS–); and 5.1 > P_e (10^{-6} cm s^{-1}) > 2.1 for compounds with uncertain BBB permeation (CNS+/–). All the tetrahydrobenzo[*h*][1,6]naphthyridine–6-chlorotacrine hybrids, **5a–d**, were predicted to be able to cross the BBB. The measured P_e values for **5a–d** were found to slightly increase with the tether length, and hence, with lipophilicity, and were clearly above the threshold for high BBB permeation (Table 1), thereby anticipating their ability to enter the brain and reach their different CNS targets.

Of note, the predicted *in vitro* ability of the novel hybrids to cross the BBB was also confirmed through the BBB permeation index obtained using a recently reported *in silico* multiclassification method (Table 2), which was developed utilizing a comprehensive data set containing around 12000 diverse compounds [29]. This method was also used to assess the intestinal absorption of the novel compounds, which was predicted to be positive in all cases. Finally, the predicted rat acute toxicity of the hybrids was clearly lower than that predicted for the anti-Alzheimer AChE inhibitor tacrine, thereby supporting the safety of these compounds (Table 2).

3. Conclusion

In this work we have further advanced in the hit-to-lead optimization process that, starting from the 3,4-dihydro-2*H*-pyrano[3,2-*c*]quinoline carboxylic ester **1**, had led to the potent hAChE inhibitors **3** [9] and **4** [10] by molecular hybridization with 6-chlorotacrine and by double O → NH bioisosteric replacement, respectively. Herein, combination of the optimized AChE PAS-binding moiety present in **4**, molecular hybridization with 6-chlorotacrine, and a MD-driven optimization of the tether length has led to the discovery of the 1,2,3,4-tetrahydrobenzo[*h*][1,6]naphthyridine–6-chlorotacrine hybrid **5a** as a picomolar inhibitor of hAChE.

Apart from **5a**, other three longer homologues, i.e. **5b–d**, have been also synthesized and found to be potent inhibitors of hAChE, exhibiting IC_{50} values in the low nanomolar range. Like the parent compounds 6-chlorotacrine, **2**, and the tetrahydrobenzo[*h*][1,6]naphthyridine **4**, hybrids **5a–d** have been found to be selective for hAChE *vs.* hBChE inhibition, albeit still keeping a potent hBChE inhibitory activity. Very interestingly, these hybrids turned out to be moderately potent dual inhibitors of Aβ42 and tau aggregation in intact *E. coli* cells, with IC_{50} values in the low micromolar range. Taking into account all the tested activities, hybrid **5d**, with the most potent Aβ42 and tau anti-aggregating activities, is likely the hybrid of the series with the most interesting multitarget profile. Notwithstanding that better balanced potencies at their different targets would have been desirable, the multitarget profile of the novel hybrids, together with their predicted ability to cross the BBB, make them interesting anti-Alzheimer lead compounds.

4. Experimental part

4.1. Chemistry. General methods.

Melting points were determined in open capillary tubes with a MFB 595010M Gallenkamp melting point apparatus. Recrystallization solvents from which the analytical samples have been obtained are indicated after the melting points. 400 MHz ^{1}H NMR and 500 MHz ^{1}H/125.8 MHz ^{13}C NMR spectra were recorded on Varian Gemini 400 and Varian Mercury 500 spectrometers, respectively. The chemical shifts are reported in ppm (δ scale) and coupling constants are reported in Hertz (Hz). Assignments given for the NMR spectra of the new compounds have been carried out by comparison with the NMR data of the precursor ester **6** and the hybrid compound **5d** which in turn, were assigned on the basis of DEPT, COSY ^{1}H/^{1}H (standard procedures), and COSY ^{1}H/^{13}C (gHSQC or gHMBC sequences) experiments. IR spectra were run on a Perkin-Elmer Spectrum RX I spectrophotometer, using the Attenuated Total Reflectance (ATR) technique. Absorption values are expressed as wave-numbers (cm^{-1}); only significant absorption bands are given. Column chromatography was performed on silica gel 60 AC.C (35–70 μM, SDS, ref 2000027). Thin-layer chromatography was performed with aluminum-backed sheets with silica gel 60 F_{254} (Merck, ref 1.05554), and spots were visualized with UV light and 1% aqueous solution of $KMnO_4$. NMR spectra of all of the new compounds were performed at the Centres Científics i Tecnològics of the University of Barcelona (CCiTUB), while elemental analyses and high resolution mass spectra were carried out at the Microanalysis Service of the IIQAB (CSIC, Barcelona, Spain) with a Carlo Erba model 1106 analyzer, and at the CCiTUB with a LC/MSD-TOF Agilent Technologies spectrometer, respectively. The HPLC measurements were performed using a HPLC Waters Alliance HT apparatus comprising a pump (Edwards RV12) with degasser, an autosampler, a diode array detector and a column as specified below. The reverse phase HPLC determinations were carried out on a YMC-Pack ODS-AQ column (50×4.6 mm, D S. 3 μm, 12 nm). Solvent A: water with 0.1% formic acid; Solvent B: acetonitrile with 0.1% formic acid, or solvent A: water with NH_4HCO_3, 10 mM pH 9.0; Solvent B: acetonitrile. Gradient: 5% of B to 100% of B within 3.5 min. Flux: 1.6 mL/min at 50 ºC. The analytical samples of all of the compounds that were subjected to pharmacological evaluation were dried at 65 ºC / 2 Torr (standard conditions) at least for 2 days and possess a purity ≥95% as evidenced by their elemental analyses and HPLC measurements. Of note, as previously reported for some tacrine-related dimeric compounds [31], the new hybrids herein described have the ability to retain molecules of water, which cannot be removed after drying the analytical samples under the aforementioned standard conditions. Thus, the elemental analyses of these compounds showed the presence of variable amounts of water, which have been indicated in the corresponding compound formulas.

4.1.1. N-{3-[(6-chloro-1,2,3,4-tetrahydroacridin-9-yl)amino]propyl}-5-(4-chlorophenyl)-1,2,3,4-tetrahydrobenzo[h][1,6]naphthyridine-9-carboxamide ***5a***

A solution of ester **6** (4.79 g, 10.2 mmol) and KOH pellets (85% purity, 2.04 g, 30.9 mmol) in MeOH (260 mL) was stirred under reflux for 24 h. The resulting mixture was cooled to room temperature and evaporated to dryness. The solid residue was treated with an Et_2O solution of HCl (1.2 N, 171 mL, 205 mmol) for 30 min and the resulting suspension was evaporated at reduced pressure, to give the corresponding tetrahydrobenzo[*h*][1,6]naphthyridinecarboxylic acid, in the form of its hydrochloride salt (6.54 g), which was directly used in the next step without further purification: IR (ATR) ν 3500–2500 (max at 3316, 2966, O–H, $^{+}$N–H, C–H st), 1679, 1584, 1574 (C=O, Ar–C–C, Ar–C–N st) cm^{-1}; ^{1}H NMR (400 MHz, CD_3SO) δ 1.28 [s, 9H, NCOO-$C(CH_3)_3$], 1.76 (m, 2H, 3-H_2), 2.66 (t, J= 5.6 Hz, 2H, 4-H_2), 3.41 (m, 2H, 2-H_2), 7.49 (d, J≈8.4 H, 2H), 7.64 (d, J=8.4 H, 2H) [2(6)-H and 3(5)-H 4-chlorophenyl], 7.78 (d, J=8.8 Hz, 1H, 7-H), 8.17 (br d, J≈8.8 Hz, 1H, 8-H), 8.34 (br s, 1H, 10-H); HRMS (ESI), calcd for [$C_{24}H_{23}{}^{35}ClN_2O_4 + H^+$] 439.1419, found 439.1410.

To a solution of crude tetrahydrobenzo[*h*][1,6]naphthyridinecarboxylic acid (298 mg) in EtOAc / DMF 10:1 (21 mL), Et_3N (0.19 mL, 138 mg, 1.36 mmol), EDC (146 mg, 0.94 mmol), and HOBt (128 mg, 0.94 mmol) were added, and the mixture was stirred at room temperature for 5 min. To the resulting mixture, amine **7a** (200 mg, 0.69 mmol) was added and the reaction mixture was stirred at room temperature for 18 h and concentrated at reduced pressure, to give a semisolid residue (1.18 g), which was purified by column chromatography (35–70 µm silica gel, CH_2Cl_2/MeOH/50% aq. NH_4OH mixtures, gradient elution). On elution with CH_2Cl_2/MeOH/50% aq. NH_4OH 99.5:0.5:0.2 to 99.2:0.8:0.2, N^1-Boc-protected amide (141 mg, 43% overall yield from **6**) and the final amide **5a** (111 mg, 39% overall yield from **6**) were successively isolated as yellowish solids.

A solution of the N^1-Boc-protected amide (141 mg, 0.20 mmol) in 4 M HCl / dioxane (2.41 mL, 9.64 mmol) was stirred thoroughly at room temperature for 18 h, and was evaporated at reduced pressure. The resulting solid residue was diluted with H_2O (3 mL) and alkalinized with 10% aqueous Na_2CO_3 (2 mL). The alkaline solution was extracted with $CHCl_3$ / MeOH 9:1 (4×25 mL) and the combined organic extracts were dried over anhydrous Na_2SO_4, and evaporated at reduced pressure to give amide **5a** (115 mg, 41% overall yield from **6**, 80% total overall yield of **5a**) as a yellowish solid; R_f 0.65 (CH_2Cl_2/MeOH/50% aq. NH_4OH 9:1:0.05).

A solution of amide **5a** (95 mg, 0.16 mmol) in MeOH (5 mL) was filtered through a 0.45 μm PTFE filter and treated with a methanolic solution of HCl (0.53 N, 2.6 mL, 1.38 mmol). The resulting solution was evaporated at reduced pressure and the solid was washed with pentane to give, after drying under standard conditions, **5a**·2HCl (95 mg) as a yellowish solid: mp 295–297 ºC (MeOH); IR (ATR) *ν* 3500–2500 (max at 3315, 3231, 3084, 3034, 2941, 2865, 2772, N–H, $^{+}$N–H, C–H st), 1643, 1632, 1578, 1553, 1514 (C=O, Ar–C–C, Ar–C–N st) cm^{-1}; ^{1}H NMR (500 MHz, CD_3OD) δ 1.94–2.02 (complex signal, 4H, 2”-H_2, 3”-H_2), superimposed in part 2.00 (tt, *J*≈*J’*≈ 6.0 Hz, 2H, 3-H_2), 2,20 (tt, *J*≈*J’*≈6.5 Hz, 2H, 2’-H_2), 2.76 (t, *J*≈6.0 Hz, 2H, 4-H_2), superimposed in part 2.78 (m, 2H, 1”-H_2), 2,99 (t, *J*=6.5 Hz, 2H, 4”-H_2), 3.61 (t, *J*=6.5 Hz, 2H, 1’-H_2), 3.73 (t, *J*=6.0 Hz, 2H, 2-H_2), 4.13 (t, *J*=6.5 Hz, 2H, 3’-H_2), 4.85 (s, NH, $^{+}$NH), 7.47 (dd, *J*=9.0 Hz, *J’*=2.0 Hz, 1H, 7”-H), 7.64 (d, *J*=2.0 Hz, 1H, 5”-H), 7.65 (dm, *J*≈9.0 Hz, 2H) and 7.68 (dm, *J*=9.0 Hz, 2H) [2(6)-H and 3(5)-H 4-chlorophenyl], 7.85 (d, *J*=8.5 Hz, 1H, 7-H), 8.20 (dd, *J*=8.5 Hz, *J’*=1.5 Hz, 1H, 8-H), 8.41 (d, *J*≈9.0 Hz, 1H, 8”-H), 8.96 (d, *J*=1.5 Hz, 1H, 10-H); ^{13}C NMR (125.8 MHz, CD_3OD) δ 20.0 (CH_2, C3), 21.7 (CH_2, C3”), 22.9 (CH_2, C2”), 24.9 (CH_2, C1”), 25.0 (CH_2, C4), 29.4 (CH_2, C4”), 31.1 (CH_2, C2’), 37.9 (CH_2, C1’), 43.0 (CH_2, C2), 46.3 (CH_2, C3’), 110.0 (C, C4a), 113.7 (C, C9a”), 115.5 (C, C8a”), 116.1 (C, C10a) 119.0 (CH, C5”), 121.0 (CH, C7), 123.8 (CH, C10), 126.7 (CH, C7”), 128.7 (CH, C8”), 130.5 (2CH) and 131.8 (2CH) [C2(6) and C3(5) 4-chlorophenyl], 132.3 (C, C1 4-chlorophenyl), 132.5 (CH, C8), 132.8 (C, C9), 138.3 (C, C4 4-chlorophenyl), 139.9 (C, C6”), 140.3 (C, C6a), 140.4 (C, C10a”), 151.6 (C, C5), 152.3 (C, C4a”), 155.8 (C, C10b), 158.2 (C, C9”), 168.2 (C, CONH); HRMS (ESI), calcd for $[C_{35}H_{33}{}^{35}Cl_2N_5O + H^+]$ 610.2135, found 610.2129; Anal. $C_{35}H_{33}Cl_2N_5O\cdot 2HCl\cdot 1.5H_2O$ (C, H, N).

*4.1.2. N-{4-[(6-chloro-1,2,3,4-tetrahydroacridin-9-yl)amino]butyl}-5-(4-chlorophenyl)-1,2,3,4-tetrahydrobenzo[h][1,6]naphthyridine-9-carboxamide **5b***

It was prepared as described for **5a**. Starting from crude tetrahydrobenzo[*h*][1,6]naphthyridinecarboxylic acid (570 mg) and amine **7b** (401 mg, 1.32 mmol), a semisolid residue (2.54 g) was obtained and purified by column chromatography (35–70 µm silica gel, CH_2Cl_2/MeOH/50% aq. NH_4OH mixtures, gradient elution). On elution with CH_2Cl_2/MeOH/50% aq. NH_4OH 99:1:0.2, N^1-Boc-protected amide (307 mg, 48% overall yield from **6**) and a 1:1 mixture of this amide with starting amine **7b** (^{1}H NMR) (234 mg, 18% overall yield of the protected amide from **6**; 66% total overall yield of protected amide from **6**) were successively isolated. Treatment of the N^1-Boc-protected amide (272 mg, 0.38 mmol) with 4 M HCl / dioxane (2.51 mL, 10.0 mmol) as described for **5a** afforded amide **5b** (237 mg, 66% overall yield from **6**) as a yellowish solid; R_f 0.67 (CH_2Cl_2/MeOH/50% aq. NH_4OH 9:1:0.05). A solution of amide **5b** (237 mg, 0.38 mmol) in CH_2Cl_2 (10 mL) was filtered through a 0.45 µm PTFE filter and treated with a methanolic solution of HCl (0.53 N, 6.3 mL, 3.34 mmol). The resulting solution was evaporated at reduced pressure and the solid was washed with pentane to give, after drying under standard conditions, **5b**·2HCl (285 mg) as a yellowish solid: mp 276–279 ºC (CH_2Cl_2/MeOH 5:3); IR (ATR) ν 3500–2500 (max. at 3226, 3062, 3028, 2937, 2871, 2803, N–H, $^+$N–H, C–H st), 1651, 1632, 1586, 1573, 1538 (C=O, Ar–C–C, Ar–C–N st) cm^{-1}; ^{1}H NMR (500 MHz, CD_3OD) δ 1.84 (tt, J≈J'≈7,0 Hz, 2H, 2'-H_2), 1,92–2,03 (complex signal, 8H, 3-H_2, 3'-H_2, 2"-H_2 and 3"-H_2), 2,71 (t, J=6.0 Hz, 2H, 1"-H_2), 2.76 (t, J=6.0 Hz, 2H, 4-H_2), 2.98 (t, J=6.0 Hz, 2H, 4"-H_2), 3,52 (t, J=7.0 Hz, 2H, 1'-H_2), 3.72 (t, J=6.0 Hz, 2H, 2-H_2), 4.05 (t, J=7.0 Hz, 2H, 4'-H_2), 4.85 (s, NH, $^+$NH), 7.50 (dd, J=9.5 Hz, J'=2.5 Hz, 1H, 7"-H), 7.66–7.70 [complex signal, 5H, 2(6)-H and 3(5)-H 4-chlorophenyl, and 5"-H], 7.84 (d, J≈9.0 Hz, 1H, 7-H), 8.22 (dd, J=9.0 Hz, J'=2.0 Hz, 1H, 8-H), 8.40 (d, J=9.5 Hz, 1H, 8"-H), 8.98 (d, J≈2.0 Hz, 1H, 10-H); ^{13}C NMR (125.8 MHz, CD_3OD) δ 20.0 (CH_2, C3), 21.7 (CH_2, C3"), 22.9 (CH_2, C2"), 24.7 (CH_2, C1"), 25.0 (CH_2, C4), 27.3 (CH_2) and 28.7 (CH_2) C2', C3'), 29.3 (CH_2, C4"), 40.7 (CH_2, C1'), 43.0 (CH_2, C2), 48.8 (CH_2, C4'), 109.9 (C, C4a), 113.6 (C, C9a"), 115.5 (C, C8a"), 116.2 (C, C10a), 119.0 (CH, C5"), 120.9 (CH, C7), 123.7 (CH, C10), 126.8 (CH, C7"), 128.9 (CH, C8"), 130.4 (2CH) and 131.8 (2CH) [C2(6) and C3(5) 4-chlorophenyl], 132.3 (C, C1 4-chlorophenyl), 132.5 (CH, C8), 133.2 (C, C9), 138.3 (C, C4 4-chlorophenyl), 140.0 (C, C6"), 140.3 (C, C6a), 140.5 (C, C10a"), 151.6 (C, C5), 152.1 (C, C4a"), 155.7 (C, C10b), 157.9 (C, C9"), 167.9 (C, CONH); HRMS (ESI), calcd for [$C_{36}H_{35}{}^{35}Cl_2N_5O + H^+$] 624.2291, found 624.2274; Anal. $C_{36}H_{35}Cl_2N_5O\cdot 2HCl\cdot 1.5H_2O$ (C, H, N).

4.1.3. N-{5-[(6-chloro-1,2,3,4-tetrahydroacridin-9-yl)amino]pentyl}-5-(4-chlorophenyl)-1,2,3,4-tetrahydrobenzo[h][1,6]naphthyridine-9-carboxamide ***5c***

It was prepared as described for **5a**. Starting from crude tetrahydrobenzo[*h*][1,6]naphthyridinecarboxylic acid (190 mg) and amine **7c** (141 mg, 0.44 mmol), a semisolid residue (1.34 g) was obtained and purified by column chromatography (35–70 µm silica gel, CH_2Cl_2/MeOH/50% aq. NH_4OH mixtures, gradient elution). On elution with CH_2Cl_2/MeOH/50% aq. NH_4OH 99.2:0.8:0.2 to 99:1:0.2, impure N^1-Boc-protected amide (51 mg) and deprotected amide **5c** (65 mg, 34% overall yield from **6**) were successively isolated as yellowish solids; R_f 0.71 (CH_2Cl_2/MeOH/50% aq. NH_4OH 9:1:0.05).

A solution of amide **5c** (65 mg, 0.10 mmol) in CH_2Cl_2 (10 mL) was filtered through a 0.45 µm PTFE filter and treated with a methanolic solution of HCl (0.53 N, 1.6 mL, 0.85 mmol). The resulting solution was evaporated at reduced pressure and the solid was washed with pentane to give, after drying under standard conditions, **5c**·2HCl (32 mg) as a yellowish solid: mp 207–208 ºC (CH_2Cl_2/MeOH 20:3); IR (ATR) ν 3500–2500 (max. at 3376, 3062, 2927, 2860, N–H, $^+$N–H, C–H st), 1625, 1614, 1587, 1541, 1519 (C=O, Ar–C–C, Ar–C–N st) cm^{-1}; ^{1}H NMR (500 MHz, CD_3OD) δ 1.30 (m, 2H, 3'-H_2), 1.58 (tt, $J \approx J' \approx$6.5 Hz, 2H, 2'-H_2), 1.77 (m, 2H, 4'-H_2), 1.90–2.02 (complex signal, 4H, 2"-H_2, 3"-H_2), superimposed in part 1.99 (tt, $J \approx J' \approx$5.0 Hz, 2H, 3-H_2), 2.69 (m, 2H, 1"-H_2), 2.76 (t, J=6.0 Hz, 2H, 4-H_2), 2.98 (m, 2H, 4"-H_2), 3.49 (td, J=7.0 Hz, J'=6.5 Hz, 2H, 1'-H_2), 3.72 (t, J=5.0 Hz, 2H, 2-H_2), 3.98 (t, J=7.0 Hz, 2H, 5'-H_2), 4.84 (s, NH, $^+$NH), 7.50 (br d, $J \approx$9.0 Hz, 1H, 7"-H), 7.66–7.72 [complex signal, 4H, 2(6)-H and 3(5)-H 4-chlorophenyl], 7.73 (d, J=1.5 Hz, 1H, 5"-H), 7.86 (d, J=9.0 Hz, 1H, 7-H), 8.24 (d, J=9.0 Hz, 1H, 8-H), 8.39 (d, J=9.0 Hz, 1H, 8"-H), 8.66 (m, 1H, CONH), 9.02 (br s, 1H, 10-H); ^{13}C NMR (125.8 MHz, CD_3OD) δ 20.0 (CH_2, C3), 21.7 (CH_2, C3"), 22.9 (CH_2, C2"), 24.9 (CH_2, C1"), 25.0 (CH_2, C4), 25.6 (CH_2, C3'), 29.4 (CH_2, C4"), 29.9 (CH_2) and 30.9 (CH_2) (C2', C4'), 40.8 (CH_2, C1'), 43.0 (CH_2, C2), 49.0 (CH_2, C5'), 109.8 (C, C4a), 113.4 (C, C9a"), 115.5 (C, C8a"), 116.1 (C, C10a), 119.0 (CH, C5"), 120.9 (CH, C7), 123.6 (CH, C10), 126.8 (CH, C7"), 128.7 (CH, C8"), 130.4 (2CH) and 131.9 (2CH) [C2(6) and C3(5) 4-chlorophenyl], 132.3 (C, C1 4-chlorophenyl), 132.7 (CH, C8), 133.3 (C, C9), 138.3 (C, C4 4-chlorophenyl), 140.0 (C, C6"), 140.2 (C, C6a), 140.4 (C, C10a"), 151.5 (C, C5), 152.2 (C, C4a"), 155.7 (C, C10b), 157.8 (C, C9"), 167.9 (C, CONH), an extra peak at 40.1 ppm was observed; HRMS (ESI), calcd for

[$C_{37}H_{37}{}^{35}Cl_2N_5O + H^+$] 638.2448, found 638.2435; Anal. $C_{37}H_{37}Cl_2N_5O \cdot 2HCl \cdot 3H_2O$ (C, H, N).

4.1.4. N-{8-[(6-chloro-1,2,3,4-tetrahydroacridin-9-yl)amino]octyl}-5-(4-chlorophenyl)-1,2,3,4-tetrahydrobenzo[h][1,6]naphthyridine-9-carboxamide ***5d***

It was prepared as described for **5a**. Starting from crude tetrahydrobenzo[*h*][1,6]naphthyridinecarboxylic acid (480 mg) and amine **7d** (400 mg, 1.11 mmol), a semisolid residue (2.45 g) was obtained and purified by column chromatography (35–70 μm silica gel, CH_2Cl_2/MeOH/50% aq. NH_4OH mixtures, gradient elution). On elution with CH_2Cl_2/MeOH/50% aq. NH_4OH 100:0:1, N^1-Boc-protected amide (370 mg, 63% overall yield from **6**) was isolated as a yellowish solid. Treatment of the N^1-Boc-protected amide (370 mg, 0.47 mmol) with 4 M HCl / dioxane (3.10 mL, 12.4 mmol) as described for **5a** afforded amide **5d** (359 mg, 63% overall yield from **6**) as a yellowish solid; R_f 0.78 (CH_2Cl_2/MeOH/50% aq. NH_4OH 9:1:0.05). A solution of amide **5d** (359 mg, 0.53 mmol) in CH_2Cl_2 (10 mL) was filtered through a 0.45 μm PTFE filter and treated with a methanolic solution of HCl (0.53 N, 8.73 mL, 4.63 mmol). The resulting solution was evaporated at reduced pressure and the solid was washed with pentane to give, after drying under standard conditions, **5d**·2HCl (283 mg) as a yellowish solid: mp 203–204 ºC (CH_2Cl_2/MeOH 5:4); IR (ATR) ν 3500–2500 (max. at 3228, 3039, 2929, 2860, N–H, $^+$N–H, C–H st), 1731, 1631, 1573 (C=O, Ar–C–C, Ar–C–N st) cm^{-1}; ^{1}H NMR (500 MHz, CD_3OD) δ 1.38–1.50 (complex signal, 8H, 3’-H_2, 4’-H_2, 5’-H_2, 6’-H_2), 1.69 (tt, *J*≈*J’*≈7.5 Hz, 2H, 2’-H_2), 1.85 (tt, *J*≈*J’*≈7.5 Hz, 2H, 7’-H_2), 1.92–2.00 (complex signal, 6H, 3-H_2, 2”-H_2, 3”-H_2), 2.68 (t, *J*=6.0 Hz, 2H, 1”-H_2), 2.75 (t, *J*=6.5 Hz, 2H, 4-H_2), 3.01 (t, *J*=6.0 Hz, 2H, 4”-H_2), 3.43 (t, *J*=7.5 Hz, 2H, 1’-H_2), 3.71 (t, *J*=6.0 Hz, 2H, 2-H_2), 3.95 (t, *J*=7.5 Hz, 2H, 8’-H_2), 4.85 (s, NH, $^+$NH), 7.55 (dd, *J*=9.5 Hz, *J’*=2.0 Hz, 1H, 7”-H), 7.67 [complex signal, 4H, 2(6)-H and 3(5)-H 4-chlorophenyl], 7.78 (d, *J*=2.0 Hz, 1H, 5”-H), 7.87 (d, *J*=9.0 Hz, 1H, 7-H), 8.25 (dd, *J*=9.0 Hz, *J’*=2.0 Hz, 1H, 8-H), 8.38 (d, *J*=9.5 Hz, 1H, 8”-H), 8.99 (d, *J*≈2.0 Hz, 1H, 10-H); ^{13}C NMR (125.8 MHz, CD_3OD) δ 20.0 (CH_2, C3), 21.8 (CH_2, C3”), 22.9 (CH_2, C2”), 24.8 (CH_2, C1”), 25.0 (CH_2, C4), 27.6 (CH_2, C6’), 28.0 (CH_2, C3’), 29.3 (CH_2, C4”), 30.1 (CH_2) and 30.2 (CH_2) (C4’, C5’), 30.4 (CH_2, C2’), 31.3 (CH_2, C7’), 41.3 (CH_2, C1’), 43.0 (CH_2, C2), 49.2 (CH_2, C8’), 109.8 (C, C4a), 113.3 (C, C9a”), 115.4 (C, C8a”), 116.1 (C, C10a), 119.1 (CH, C5”), 120.9 (CH, C7), 123.6 (CH, C10), 126.7 (CH, C7”), 128.8 (CH, C8”), 130.4 (2CH) and 131.9 (2CH) [C2(6) and C3(5) 4-

chlorophenyl], 132.2 (C, C1 4-chlorophenyl), 132.6 (CH, C8), 133.5 (C, C9), 138.3 (C, C4 4-chlorophenyl), 140.1 (C, C6”), 140.2 (C, C6a), 140.5 (C, C10a”), 151.4 (C, C5), 152.1 (C, C4a”), 155.7 (C, C10b), 157.8 (C, C9”), 167.9 (C, CONH); HRMS (ESI), calcd for [$C_{40}H_{43}{}^{35}Cl_2N_5O + H^+$] 680.2917, found 680.2900; Anal. $C_{40}H_{43}Cl_2N_5O \cdot 2HCl \cdot 2.5H_2O$ (C, H, N).

4.2. Biological assays

4.2.1. Determination of AChE and BChE inhibitory activities

The inhibitory activities against human recombinant AChE (Sigma-Aldrich) and human serum BChE (Sigma-Aldrich) were evaluated spectrophotometrically by the method of Ellman *et al.* [15]. The reactions took place in a final volume of 300 μL of 0.1 M phosphate-buffered solution pH 8.0, containing hAChE (0.02 u/mL) or hBChE (0.02 u/mL) and 333 μM 5,5'-dithiobis(2-nitrobenzoic) acid (DTNB; Sigma-Aldrich) solution used to produce the yellow anion of 5-thio-2-nitrobenzoic acid. Inhibition curves were performed in duplicates using at least 10 increasing concentrations of inhibitors and preincubated for 20 min at 37 ºC before adding the substrate [32]. One duplicate sample without inhibitor was always present to yield 100% of AChE or BChE activities. Then substrates, acetylthiocholine iodide (450 μM; Sigma-Aldrich) or butyrylthiocholine iodide (300 μM; Sigma-Aldrich), were added and the reaction was developed for 5 min at 37 ºC. The colour production was measured at 414 nm using a labsystems Multiskan spectrophotometer.

Data from concentration–inhibition experiments of the inhibitors were calculated by non-linear regression analysis, using the GraphPad Prism program package (GraphPad Software; San Diego, USA), which gave estimates of the IC_{50} (concentration of drug producing 50% of enzyme activity inhibition). Results are expressed as mean ± S.E.M. of at least 4 experiments performed in duplicate.

4.2.2. Determination of Aβ42 and tau aggregation inhibitory activities in intact Escherichia coli cells

Cloning and overexpression of Aβ42 peptide: Escherichia coli competent cells BL21 (DE3) were transformed with the pET28a vector (Novagen, Inc., Madison, WI, USA) carrying the DNA sequence of Aβ42. Because of the addition of the initiation codon ATG in front of both genes, the overexpressed peptide contains an additional methionine residue at its N terminus. For overnight culture preparation, 10 mL of lysogeny broth (LB) medium containing 50 μg·mL^{-1} of kanamycin were inoculated with a colony of BL21 (DE3) bearing the plasmid to be expressed at 37 °C. After overnight growth, the OD600 was usually 2–2.5. For expression of Aβ42 peptide, 20 μL of overnight culture were transferred into eppendorf tubes of 1.5 mL containing 960 μL of LB medium with 50 μg·mL^{-1} of kanamycin, 1 mM of isopropyl 1-thio-β-D-galactopyranoside (IPTG), 10 μL of a 10 μM solution of each hybrid **5** or reference compound in DMSO, and 10 μL of a 25 μM solution of Th-S in water. The samples were grown for 24 h at 37 °C and 1400 rpm using a Thermomixer (Eppendorf, Hamburg, Germany). In the negative control (without drug) the same amount of DMSO was added in the sample.

Cloning and overexpression of tau protein: E. coli BL21 (DE3) competent cells were transformed with pTARA containing the RNA-polymerase gen of T7 phage (T7RP) under the control of the promoter pBAD. *E. coli* BL21 (DE3) with pTARA competent cells were transformed with pRKT42 vector encoding four repeats of tau protein in two inserts. For overnight culture preparation, 10 mL of M9 medium containing 0.5% of glucose, 50 μg·mL^{-1} of ampicillin and 12.5 μg·mL^{-1} of chloramphenicol were inoculated with a colony of BL21 (DE3) bearing the plasmids to be expressed at 37 °C. After overnight growth, the OD600 was usually 2–2.5. For expression of tau protein, 20 μL of overnight culture were transferred into eppendorf tubes of 1.5 mL containing 970 μL of M9 medium containing 0.25% of arabinose, 0.5% of glucose, 50 μg·mL^{-1} of ampicillin and 12.5 μg·mL^{-1} of chloramphenicol, 10 μL of a 10 μM solution of each hybrid **5** or reference compound in DMSO, and 10 μL of a 25 μM solution of Th-S in water. The samples were grown for 24 h at 37 °C and 1400 rpm using a Thermomixer (Eppendorf, Hamburg, Germany). In the negative control (without drug) the same amount of DMSO was added in the sample.

Th-S steady-state fluorescence: Th-S (T1892) and other chemical reagents were purchased from Sigma (St. Louis, MO). Th-S stock solution (2.5 mM) was prepared in double-distilled water purified through a Milli-Q system (Millipore, USA). Fluorescent spectral scans of Th-S were analyzed using an Aminco Bowman Series 2 luminescence spectrophotometer (Aminco-Bowman AB2, SLM Aminco, Rochester, NY, USA). Excitation and emission slit widths of 4 nm were used. Finally, the fluorescence emission at 455 nm, when exciting at 375 nm, was recorded. In order to normalize the Th-S fluorescence as a function of the bacterial concentration, OD_{600} was obtained using a Shimadzu UV-2401 PC UV–Vis spectrophotometer (Shimadzu, Japan). The final fluorescence data were obtained considering as 100% the Th-S fluorescence of the bacterial cells expressing the peptide or protein in the absence of drug and 0% the Th-S fluorescence of the bacterial cells non-expressing the peptide or protein. Final data are the average of ten independent experiments.

4.2.3. PAMPA-BBB assay

To evaluate the brain penetration of hybrids **5**, a parallel artificial membrane permeation assay for blood–brain barrier was used, following the method described by Di *et al.* [28]. The *in vitro* permeability (P_e) of fourteen commercial drugs through lipid extract of porcine brain membrane together with the test compounds was determined. Commercial drugs and the synthesized compounds were tested using a mixture PBS:EtOH 70:30. Assay validation was made by comparing the experimental permeability of the different compounds with the reported bibliography values of the commercial drugs, which showed a good correlation: P_e (exp) = 1.5010 P_e (lit) – 0.8618 (R^2 = 0.9199). From this equation and taking into account the limits established by Di *et al.* for BBB permeation, we established the ranges of permeability as compounds of high BBB permeation (CNS+): P_e (10^{-6} cm s^{-1}) > 5.1; compounds of low BBB permeation (CNS–): P_e (10^{-6} cm s^{-1}) < 2.1, and compounds of uncertain BBB permeation (CNS+/–): 5.1 > P_e (10^{-6} cm s^{-1}) > 2.1.

4.3. Molecular modelling

4.3.1. Setup of the system. Molecular modelling was performed using the X-ray crystallographic structure of hAChE in complex with huprine W (PDB ID: 4BDT [15]). The structure was refined by removal of *N*-acetyl-D-glucosamine and sulphate anions and addition of missing hydrogen atoms. The enzyme was modelled in its physiological active form with neutral His447 and deprotonated Glu334, which together with Ser203 form the catalytic triad. The ionization state for the rest of ionizable residues was assessed from PROPKA3 [33] calculations. Accordingly, the standard ionization state at neutral pH was considered but for residues Glu285, Glu450 and Glu452, which were protonated. Finally, three disulfide bridges were defined between Cys residues 257–272, 529–409, and 69–96, respectively.

4.3.2. Molecular dynamics simulations. The binding mode of hybrid **5a** to hAChE was explored by means of MD simulations. Starting from that proposed initial pose, a 100 ns MD simulation was performed using the PMEMD module of AMBER12 [34] software package, the parm99SB [35] force field for the protein and the GAFF-derived parameters [36] for the ligand, whose geometrical parameters were optimized at the B3LYP/6-31G(d) level [37] and its charge distribution was described by using electrostatic potential charges with the RESP procedure [38]. Na^+ cations were added to neutralize the negative charge of the system with the XLEAP module of AMBER12. The system was immersed in an octahedral box of TIP3P [39] water molecules, preserving the crystallographic waters inside the binding cavity. The final system contained around 52000 atoms.

The geometry of the system was minimized in four steps. First, water molecules and counterions were refined through 7000 steps of conjugate gradient and 3000 steps of steepest descent algorithm. Then, the position of hydrogen atoms was optimized using 4500 steps of conjugate gradient and 500 steps of steepest descent algorithm. At the third stage, hydrogen atoms, water molecules and counterions were further optimized using 11500 steps of conjugate gradient and 2500 steps of steepest descent algorithm. Thermalization of the system was performed in five steps of 25 ps, increasing the temperature from 50 to 298 K. Concomitantly, the residues that define the binding site were restrained during thermalization using a variable restraining force. Thus, a force constant of 25 kcal mol $^{-1}$Å^{-2} was used in the first stage of the thermalization and was subsequently decreased by increments of 5 kcal mol $^{-1}$Å^{-2} in the next stages. Then, an additional step of 250 ps was performed in order to equilibrate the system density at constant pressure (1 bar) and temperature (298 K). Finally, a 100 ns trajectory was run using a time step of 2 fs. SHAKE was used for those bonds containing hydrogen atoms in conjunction with periodic boundary conditions at constant volume and temperature, particle mesh Ewald for the treatment of long electrostatic interactions, and a cutoff of 10 Å for nonbonded interactions. Moreover, in the initial 20 ns of the simulation the distance between the protonated nitrogen in the 6-chlorotacrine moiety of the inhibitor and the carbonyl oxygen of His447 was constrained to avoid artefactual rearrangements in the CAS of the enzyme.

The structural analysis was performed using in-house software and standard codes of AMBER12. The solvent interaction energies (SIE) technique developed by Purisima and co-workers [19] was used to estimate the interaction free energies for the AChE inhibitor. Calculations were performed for a set of 200 snapshots taken along the last 40 ns of the MD trajectory.

Acknowledgments

This work was supported by Ministerio de Ciencia e Innovación (MICINN) (CTQ2011-22433, CTQ2012-30930, SAF2011-27642, SAF2009-10553, start-up grant of the Ramón y Cajal program for R.S.), Generalitat de Catalunya (GC) (2009SGR1396, 2009SGR1024, 2009SGR249), and Xarxa de Recerca en Química Teòrica i Computacional (XRQTC). Fellowships from GC to O.D.P. and F.J.P.-A., a contract from the Ramón y Cajal program of MICINN to R.S., a contract from the Juan de la Cierva program of Ministerio de Economía y Competitividad to A.E., and the ICREA Academia support to F.J.L. are gratefully acknowledged. The Center for Scientific and Academic Services of Catalonia (CESCA) is acknowledged for providing access to computational facilities. We are grateful to Dr. Marc Revés and Dr. F. Spyrakis for their technical assistance in the HPLC purity measurements and in predicting safety data, respectively.

Appendix A. Supplementary material

Supplementary data related to this article can be found at http://dx.doi.org/. These data include data of the elemental analyses of hybrids **5a**–**d**, additional results from the molecular modeling studies and PAMPA-BBB assay, as well as copies of the ^{1}H and ^{13}C NMR spectra of the tested compounds.

References

[1] Alzheimer's Association, 2013 Alzheimer's disease facts and figures, Alzheimers Dementia 9 (2013) 208–245.

[2] R.E. Becker, N.H. Greig, E. Giacobini, L.S. Schneider, L. Ferruci, A new roadmap for drug development for Alzheimer's disease, Nat. Rev. Drug Discovery 13 (2014) 156.

[3] S.W. Pimplikar, Reassessing the amyloid cascade hypothesis of Alzheimer's disease, Int. J. Biochem. Cell Biol. 41 (2009) 1261–1268.

[4] (a) Y. Bansal, O. Silakari, Multifunctional compounds: Smart molecules for multifactorial diseases, Eur. J. Med. Chem. 76 (2014) 31–42;
(b) W.J. Geldenhuys, C.J. Van der Schyf, Rationally designed multi-targeted agents against neurodegenerative diseases, Curr. Med. Chem. 20 (2013) 1662–1672;

(c) X. Chen, M. Decker, Multi-target compounds acting in the central nervous system designed from natural products, Curr. Med. Chem. 20 (2013) 1673–1685;

(d) P. Russo, A. Frustaci, A. Del Bufalo, M. Fini, A. Cesario, Multitarget drugs of plants origin acting on Alzheimer's disease, Curr. Med. Chem. 20 (2013) 1686–1693;

(e) A. Rampa, F. Belluti, S. Gobbi, A. Bisi, Hybrid-based multi-target ligands for the treatment of Alzheimer's disease, Curr. Top. Med. Chem. 11 (2011) 2716–2730;

(f) A. Cavalli,; M.L. Bolognesi, A. Minarini, M. Rosini, V. Tumiatti, M. Recanatini, C. Melchiorre, Multi-target-directed ligands to combat neurodegenerative diseases, J. Med. Chem. 51 (2008) 347–372.

[5] A. Mullard, Sting of Alzheimer's failures offset by upcoming prevention trials, Nat. Rev. Drug Discovery 11 (2012) 657–660.

[6] C.R. Jack, Jr., D.M. Holtzman, Biomarker modeling of Alzheimer's disease, Neuron 80 (2013) 1347–1358.

[7] (a) N.C. Inestrosa, A. Alvarez, C.A. Pérez, R.D. Moreno, M. Vicente, C. Linker, O.I. Casanueva, C. Soto, J. Garrido, Acetylcholinesterase accelerates assembly of amyloid-β-peptides into Alzheimer's fibrils: possible role of the peripheral site of the enzyme, Neuron 16 (1996) 881–891;

(b) N.C. Inestrosa, M.C. Dinamarca, A. Alvarez, Amyloid–cholinesterase interactions. Implications for Alzheimer's disease, FEBS J. 275 (2008) 625–632;

(c) G.V. De Ferrari, M.A. Canales, I. Shin, L.M. Weiner, I. Silman, N.C. Inestrosa, A structural motif of acetylcholinesterase that promotes amyloid beta-peptide fibril formation, Biochemistry 40 (2001) 10447–10457.

[8] J.L. Sussman, M. Harel, F. Frolow, C. Oefner, A. Goldman, L. Toker, I. Silman, Atomic structure of acetylcholinesterase from Torpedo californica – a prototypic acetylcholine-binding protein, Science 253 (1991) 872–879.

[9] P. Camps, X. Formosa, C. Galdeano, D. Muñoz-Torrero, L. Ramírez, E. Gómez, N. Isambert, R. Lavilla, A. Badia, M.V. Clos, M. Bartolini, F. Mancini, V. Andrisano, M.P. Arce, M.I. Rodríguez-Franco, O. Huertas, T. Dafni, F.J. Luque, Pyrano[3,2-*c*]quinoline–6-chlorotacrine hybrids as a novel family of acetylcholinesterase- and *β*-amyloid-directed anti-Alzheimer compounds, J. Med. Chem. 52 (2009) 5365–5379.

[10] O. Di Pietro, E. Viayna, E. Vicente-García, M. Bartolini, R. Ramón, J. Juárez-Jiménez, M.V. Clos, B. Pérez, V. Andrisano, F.J. Luque, R. Lavilla, D. Muñoz-Torrero, 1,2,3,4-Tetrahydrobenzo[*h*][1,6]naphthyridines as a new family of potent peripheral-to-midgorge-site inhibitors of acetylcholinesterase: Synthesis, pharmacological evaluation and mechanistic studies, Eur. J. Med. Chem. 73 (2014) 141–152.

[11] M. Harel, I. Schalk, L. Ehret-Sabatier, F. Bouet, M. Goeldner, C. Hirth, P.H. Axelsen, I. Silman, J.L. Sussman, Quaternary ligand binding to aromatic residues in the active-site gorge of acetylcholinesterase, Proc. Natl. Acad. Sci. U.S.A. 90 (1993) 9031–9035.

[12] E. Vicente-García, F. Catti, R. Ramón, R. Lavilla, Unsaturated lactams: new inputs for Povarov-type multicomponent reactions, Org. Lett. 12 (2010) 860–863.

[13] E. Vicente-García, R. Ramón, S. Preciado, R. Lavilla, Multicomponent reaction access to complex quinolines via oxidation of the Povarov adducts, Beilstein J. Org. Chem. 7 (2011) 980–987.

[14] (a) P. Muñoz-Ruiz, L. Rubio, E. García-Palomero, I. Dorronsoro, M. del Monte-Millán, R. Valenzuela, P. Usán, C. de Austria, M. Bartolini, V. Andrisano, A. Bidon-Chanal, M. Orozco, F.J. Luque, M. Medina, A. Martínez, Design, synthesis, and biological evaluation of dual binding site acetylcholinesterase inhibitors: New disease-modifying agents for Alzheimer’s disease, J. Med. Chem. 48 (2005) 7223–7233;

(b) P.R. Carlier, Y.F. Han, E.S.-H. Chow, C.P.-L. Li, H. Wang, T.X. Lieu, H.S. Wong, Y.-P. Pang, Evaluation of short-tether bis-THA AChE Inhibitors. A further test of the dual binding site hypothesis, Bioorg. Med. Chem. 7 (1999) 351–357;

(c) M. Rosini, V. Andrisano, M. Bartolini, M.L. Bolognesi, P. Hrelia, A. Minarini, A. Tarozzi, C. Melchiorre, Rational approach to discover multipotent anti-Alzheimer drugs, J. Med. Chem. 48 (2005) 360–363.

[15] G.L. Ellman, K.D. Courtney, V. Andres Jr., R.M. Featherstone, A new and rapid colorimetric determination of acetylcholinesterase activity, Biochem. Pharmacol. 7 (1961) 88–95.

[16] (a) W.G. Lewis, L.G. Green, F. Grynszpan, Z. Radić, P.R. Carlier, P. Taylor, M.G. Finn, K.B. Sharpless, Click chemistry in situ: Acetylcholinesterase as a

reaction vessel for the selective assembly of a femtomolar inhibitor from an array of building blocks, Angew. Chem. Int. Ed. 41 (2002) 1053–1057:
(b) P. Camps, B. Cusack, W.D. Mallender, R. El Achab, J. Morral, D. Muñoz-Torrero, T. L. Rosenberry, Huprine X is a novel high-affinity inhibitor of acetylcholinesterase that is of interest for the treatment of Alzheimer’s disease, Mol. Pharmacol. 57 (2000) 409–417.

[17] F. Nachon, E. Carletti, C. Ronco, M. Trovaslet, Y. Nicolet, L. Jean, P.-Y. Renard, Crystal structures of human cholinesterases in complex with huprine W and tacrine: elements of specificity for anti-Alzheimer's drugs targeting acetyl- and butyrylcholinesterase. Biochem. J. 453 (2013) 393–399.

[18] H. Dvir, D.M. Wong, M. Harel, X. Barril, M. Orozco, F.J. Luque, D. Muñoz-Torrero, P. Camps, T.L. Rosenberry, I. Silman, J.L. Sussman, 3D Structure of *Torpedo californica* acetylcholinesterase complexed with huprine X at 2.1 Å resolution: kinetic and molecular dynamics correlates, Biochemistry 41 (2002) 2970–2981.

[19] M. Naïm, S. Bhat, K.N. Rankin, S. Dennis, S.F. Chowdhury, I. Siddiqi, P. Drabik, T. Sulea, C.I. Bayly, A. Jakalian, E.O. Purisima, Solvated interaction energy (SIE) for scoring protein−ligand binding affinities. 1. Exploring the parameter space, J. Chem. Inf. Model. 47 (2007) 122–133.

[20] R.M. Lane, S.G. Potkin, A. Enz, Targeting acetylcholinesterase and butyrylcholinesterase in dementia, Int. J. Neuropsychopharmacol. 9 (2006) 101–124.

[21] (a) E. Viayna, R. Sabate, D. Muñoz-Torrero, Dual inhibitors of β-amyloid aggregation and acetylcholinesterase as multi-target anti-Alzheimer drug candidates, Curr. Top. Med. Chem. 13 (2013) 1820–1842;
(b) B. Bulic, M. Pickhardt, B. Schmidt, E.-M. Mandelkow, H. Waldmann, E. Mandelkow, Development of tau aggregation inhibitors for Alzheimer’s disease, Angew. Chem. Int. Ed. 48 (2009) 1740–1752.

[22] S. Pouplana, A. Espargaró, C. Galdeano, E. Viayna, I. Sola, S. Ventura, D. Muñoz-Torrero, R. Sabate, Thioflavin-S staining of bacterial inclusion bodies for the fast, simple, and inexpensive screening of amyloid aggregation inhibitors. Curr. Med. Chem. 21 (2014), 1152–1159.

[23] (a) Y. Porat, A. Abramowitz, E. Gazit, Inhibition of amyloid fibril formation by polyphenols: structural similarity and aromatic interactions as a common inhibition mechanism. Chem. Biol. Drug Des. 67 (2006) 27–37;
(b) H.-Y. Zhang, Same causes, same cures. Biochem. Biophys. Res. Commun. 351 (2006) 578–581.

[24] M. Cui, Past and recent progress of molecular imaging probes for β-amyloid plaques in the brain, Curr. Med. Chem. 21 (2014) 82–112.

[25] K. Lu, Y. Jiang, B. Chen, E.M. Eldemenky, G. Ma, M. Packiarajan, G. Chandrasena, A.D. White, K.A. Jones, B. Li, S.-P. Hong, Strategies to lower the Pgp efflux liability in a series of potent indole azetidine MCHR1 antagonists. Bioorg. Med. Chem. Lett. 21 (2011) 5310–5314.

[26] (a) C.A. Lipinski, F. Lombardo, B.W. Dominy, P.J. Feeney, Experimental and computational approaches to estimate solubility and permeability in drug discovery and development settings, Adv. Drug Delivery Rev. 23 (1997) 3–25;
(b) R. Morphy, Z. Rankovic, Designing multiple ligands – medicinal chemistry strategies and challenges, Curr. Pharm. Des. 15 (2009) 587–600.

[27] (a) E. García-Palomero, P. Muñoz, P. Usan, P. Garcia, C. De Austria, R. Valenzuela, L. Rubio, M. Medina, A. Martínez, Potent β-Amyloid Modulators, Neurodegener. Dis. 5 (2008) 153–156;
(b) C. Spuch, D. Antequera, M.I. Fernandez-Bachiller, M. I. Rodríguez-Franco, E. Carro, A new tacrine–melatonin hybrid reduces amyloid burden and behavioral deficits in a mouse model of Alzheimer’s disease, Neurotox. Res. 17 (2010) 421–431;
(c) C. Galdeano, E. Viayna, I. Sola, X. Formosa, P. Camps, A. Badia, M.V. Clos, J. Relat, M. Ratia, M. Bartolini, F. Mancini, V. Andrisano, M. Salmona, C. Minguillón, G.C. González-Muñoz, M.I. Rodríguez-Franco, A. Bidon-Chanal, F.J. Luque, D. Muñoz-Torrero, Huprine–tacrine heterodimers as anti-amyloidogenic compounds of potential interest against Alzheimer’s and prion diseases, J. Med. Chem. 55 (2012) 661–669;
(d) V. Capurro, P. Busquet, J.P. Lopes, R. Bertorelli, G. Tarozzo, M.L. Bolognesi, D. Piomelli, A. Reggiani, A. Cavalli, Pharmacological characterization of memoquin, a multi-target compound for the treatment of Alzheimer’s disease, PLoS One 8 (2013) e56870;

(e) E. Viayna, I. Sola, M. Bartolini, A. De Simone, C. Tapia-Rojas, F.G. Serrano, R. Sabaté, J. Juárez-Jiménez, B. Pérez, F.J. Luque, V. Andrisano, M.V. Clos, N.C. Inestrosa, D. Muñoz-Torrero, Synthesis and multitarget biological profiling of a novel family of rhein derivatives as disease-modifying anti-Alzheimer agents, J. Med. Chem. 57 (2014) 2549–2567.

[28] L. Di, E.H. Kerns, K. Fan, O.J. McConnell, G.T. Carter, High throughput artificial membrane permeability assay for blood-brain barrier, Eur. J. Med. Chem. 38 (2003) 223–232.

[29] X. Li, L. Chen, F. Cheng, Z. wu, H. Bian, C. Xu, W. Li, G. Li, X. Shen, Y. Tang, In Silico prediction of chemical acute oral toxicity using multi-classification methods, J. Chem. Inf. Model. 54 (2014) 1061–1069.

[30] A. Villalobos, T.W. Butler, D.S. Chapin, Y.L. Chen, S.B. DeMattos, J.L. Ives, S.B. Jones, D.R. Liston, A.A. Nagel, 5,7-Dihydro-3-[2-[1-(phenylmethyl)-4-piperidinyl]ethyl]-6*H*-pyrrolo[3,2-*f*]-1,2-benzisoxazol-6-one: A potent and centrally-selective inhibitor of acetylcholinesterase, J. Med. Chem. 38 (1995) 2802–2808.

[31] F. Aguado, A. Badía, J. E. Baños, F. Bosch, C. Bozzo, P. Camps, J. Contreras, M. Dierssen, C. Escolano, D. M. Görbig, D. Muñoz-Torrero, M. D. Pujol, M. Simón, M. T. Vázquez, N. M. Vivas, Synthesis and evaluation of tacrine-related compounds for the treatment of Alzheimer’s disease, Eur. J. Med. Chem. 29 (1994) 205–221.

[32] E. Viayna, T. Gómez, C. Galdeano, L. Ramírez, M. Ratia, A. Badia, M.V. Clos, E. Verdaguer, F. Junyent, A. Camins, M. Pallàs, M. Bartolini, F. Mancini, V. Andrisano, M.P. Arce, M.I. Rodríguez-Franco, A. Bidon-Chanal, F.J. Luque, P. Camps, D. Muñoz-Torrero, Novel huprine derivatives with inhibitory activity toward β-amyloid aggregation and formation as disease-modifying anti-Alzheimer drug candidates, ChemMedChem 5 (2010) 1855–1870.

[33] M.H.M. Olsson, C.R. Sondergard, M. Rostkowski, J.H. Jensen, PROPKA3: Consistent treatment of internal and surface residues in empirical pKa predictions. J. Chem. Theory Comput. 7 (2011) 525–537.

[34] D.A. Case, T.A. Darden, T.E. Cheatham, III, C.L. Simmerling, J. Wang, R.E. Duke, R. Luo, R.C. Walker, W. Zhang, K.M. Merz, B. Roberts, S. Hayik, A. Roitberg, G. Seabra, J. Swails, A.W. Goetz, I. Kolossváry, K.F. Wong, F. Paesani, J. Vanicek, R.M. Wolf, J. Liu, X. Wu, S.R. Brozell, T. Steinbrecher, H.

Gohlke, Q. Cai, X. Ye, J. Wang, M.-J. Hsieh, G. Cui, D.R. Roe, D.H. Mathews, M.G. Seetin, R. Salomon-Ferrer, C. Sagui, V. Babin, T. Luchko, S. Gusarov, A. Kovalenko, P.A. Kollman (2012), *AMBER 12*, University of California, San Francisco.

[35] V. Hornak, R. Abel, A. Okur, B. Strockbine, A. Roitberg, C. Simmerling, Comparison of multiple Amber force fields and development of improved protein backbone parameters, Proteins 65 (2006), 712–725.

[36] J. Wang, R.M. Wolf, J.W. Caldwell, P.A. Kollman, D.A. Case, Development and testing of a general AMBER force field, J. Comput. Chem. 25 (2004) 1157–1174.

[37] (a) A.D. Becke, Density-functional thermochemistry. III. The role of exact exchange, J. Chem. Phys. 98 (1993) 5648–5652;
(b) C. Lee, W. Yang, R.G. Parr, Development of the Colle-Salvetti correlation-energy formula into a functional of the electron density, Phys. Rev. B 37 (1988) 785–789.

[38] C.I. Bayly, P. Cieplak, W.D. Cornell, P.A. Kollman, A well-behaved electrostatic potential based method using charge restraints for deriving atomic charges, J. Phys. Chem. 97 (1993) 10269–10280.

[39] W.L. Jorgensen, J. Chandrasekhar, J.D. Madura,; R.W. Impey, M.L. Klein, Comparison of simple potential functions for simulating liquid water, J. Chem. Phys. 79 (1983) 926–935.

Table, Figures, and Scheme Legends

Table 1. Inhibitory activities of 1,2,3,4-tetrahydrobenzo[*h*][1,6]naphthyridine–6-chlorotacrine hybrids and reference compounds against AChE, BChE, Aβ42 and tau aggregation, and BBB predicted permeabilities.

Table 2. *In silico* prediction of ADMET properties for hybrids **5a–d** and the reference compound tacrine.

Fig. 1. Rational design of the tetrahydrobenzo[*h*][1,6]naphthyridine–6-chlorotacrine hybrid **5a**.

Fig. 2. Superimposition of the MD-predicted binding mode of tetrahydrobenzo[*h*][1,6]naphthyridine **4** in AChE with the X-ray structure of the complex *Torpedo californica* AChE–tacrine.

Fig. 3. Representation of the binding mode of the tetrahydrobenzo[*h*][1,6]naphthyridine–6-chlorotacrine hybrid **5a** (magenta) in the average structure obtained from the snapshots sampled in the last 5 ns of the trajectory. The residues involved in interactions are shown as green-coloured sticks.

Scheme 1. Synthesis of the target tetrahydrobenzo[*h*][1,6]naphthyridine–6-chlorotacrine hybrids.

Table 1. Inhibitory activities of 1,2,3,4-tetrahydrobenzo[*h*][1,6]naphthyridine–6-chlorotacrine hybrids and reference compounds against AChE, BChE, Aβ42 and tau aggregation, and BBB predicted permeabilities.

Compd	hAChE IC_{50} (nM)[a]	hBChE IC_{50} (nM)[a]	Aβ42 aggregation in *E. coli* (% inhib. at 10 μM)[b]	Tau protein aggregation in *E. coli* (% inhib. at 10 μM)[b]	*Pe* (10^{-6} cm s^{-6})[c] (Prediction)
5a	0.006 ± 0.002	120 ± 13	52.5 ± 0.4	40.7 ± 0.5	10.5 ± 0.7 (CNS+)
5b	14.2 ± 1.7	205 ± 16	55.8 ± 0.7	58.9 ± 0.4	13.8 ± 0.4 (CNS+)
5c	14.2 ± 1.9	337 ± 30	54.3 ± 0.7	57.7 ± 0.5	14.3 ± 1.3 (CNS+)
5d	2.06 ± 0.3	286 ± 35	77.5 ± 0.9	68.7 ± 0.5	19.2 ± 1.3 (CNS+)
1	na[d]	na[d]	41.8 ± 0.4	27.9 ± 1.2	9.9 ± 1.4 (CNS+)
2	5.9 ± 0.6	114 ± 4	11.0 ± 0.6	1.4 ± 0.7	19.8 ± 0.4 (CNS+)[e]
3	19.3 ± 1.4	223 ± 35	54.6 ± 0.5	37.8 ± 0.5	13.9 ± 0.8 (CNS+)
4	65.0 ± 3.0[f]	920 ± 30[f]	nd[g]	nd[g]	22.9 ± 0.8 (CNS+)[f]

[a] IC_{50} inhibitory concentration (nM) of human recombinant AChE and human serum BChE. IC_{50} values are expressed as mean ± standard error of the mean (SEM) of at least four experiments (n = 4), each performed in duplicate.

[b] % Inhibition of Aβ42 and tau protein aggregation at 10 μM in intact *E. coli* cells. Values are expressed as mean ± SEM of four independent experiments (n = 4).

[c] Permeability values from the PAMPA-BBB assay. Values are expressed as the mean ± SD of three independent experiments (n = 3).

[d] Not active.

[e] Data from [9].

[f] Data from [10].

[g] Not determined.

Table 2. *In silico* prediction of ADMET properties for hybrids **5a–d** and the reference compound tacrine.

Compd	Blood–brain barrier permeation	Intestinal absorption	Rat acute toxicity LD_{50} (mg/kg)
5a	+	+	566
5b	+	+	449
5c	+	+	803
5d	+	+	493
Tacrine	+	+	75 (70)[a]

[a] Taken from ref. 30.

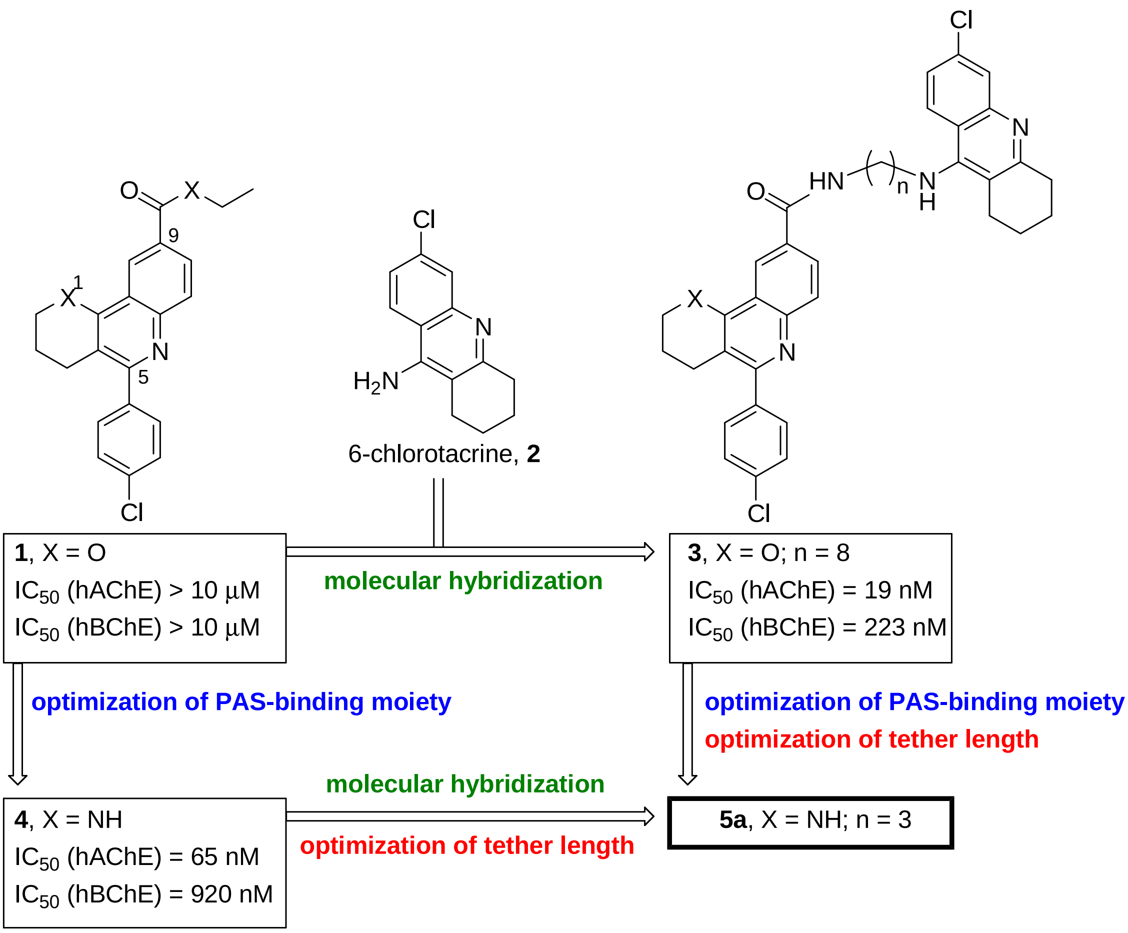
6-chlorotacrine, 2
1, X = O
IC50 (hAChE) > 10 µM
IC50 (hBChE) > 10 µM
molecular hybridization
3, X = O; n = 8
IC50 (hAChE) = 19 nM
IC50 (hBChE) = 223 nM
optimization of PAS-binding moiety
optimization of PAS-binding moiety
optimization of tether length
molecular hybridization
4, X = NH
IC50 (hAChE) = 65 nM
IC50 (hBChE) = 920 nM
optimization of tether length
5a, X = NH; n = 3

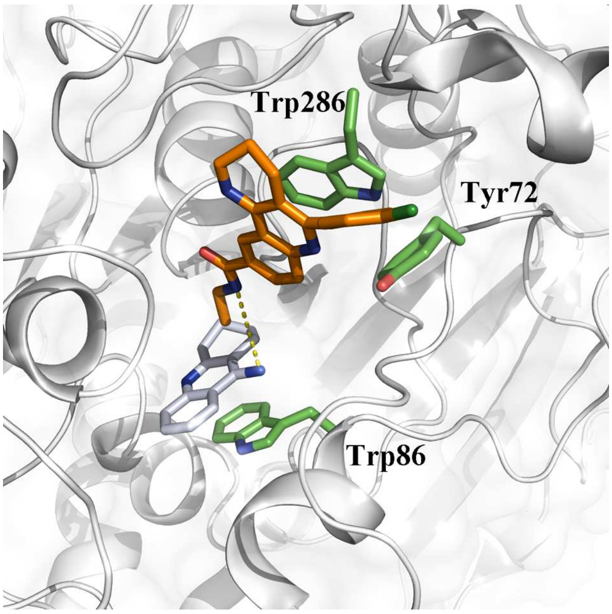
Trp286
Tyr72
Trp86

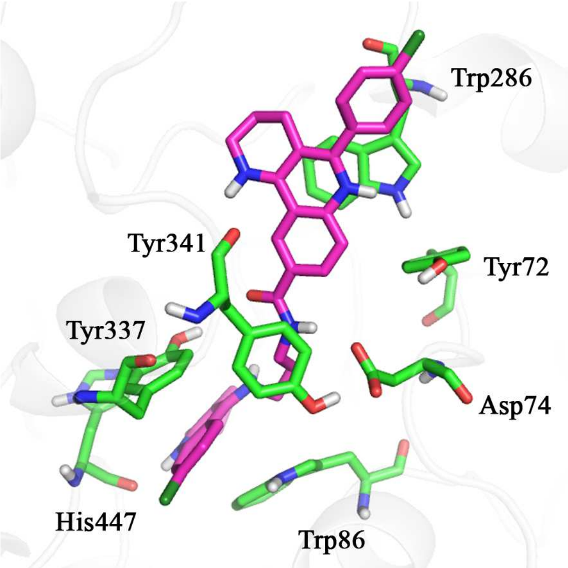
Trp286
Tyr341
Tyr72
Tyr337
Asp74
His447
Trp86

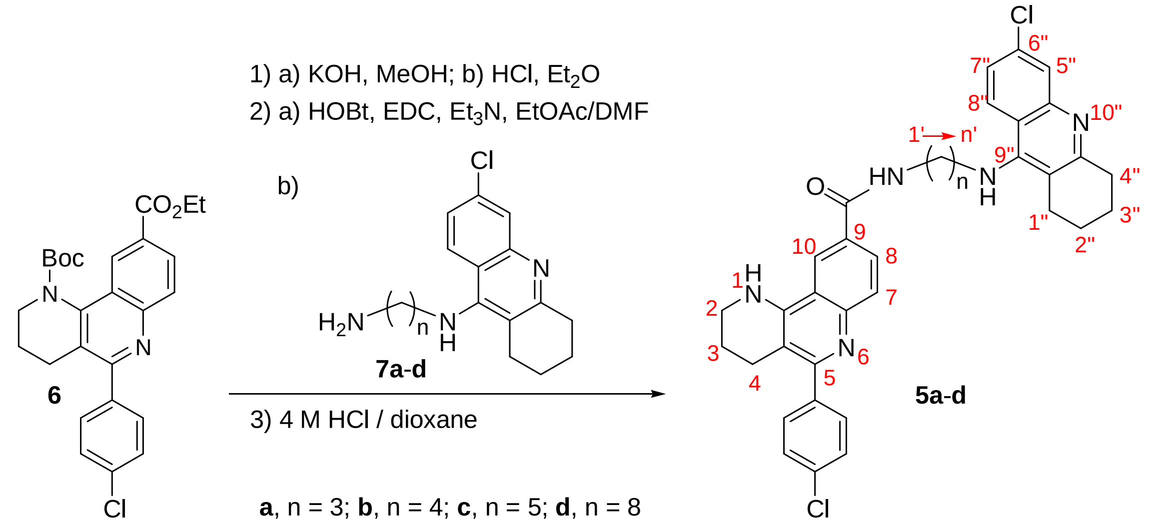
1) a) KOH, MeOH; b) HCl, Et2O
2) a) HOBt, EDC, Et3N, EtOAc/DMF
b)
7a-d
3) 4 M HCl / dioxane
a, n = 3; b, n = 4; c, n = 5; d, n = 8
6
5a-d